

## ESTIMATES OF FAST RADIO BURST DISPERSION MEASURES FROM COSMOLOGICAL SIMULATIONS

N. POL,<sup>1,2</sup> M. T. LAM,<sup>3,4</sup> M. A. McLAUGHLIN,<sup>3,4</sup> T. J. W. LAZIO,<sup>5</sup> AND J. M. CORDES<sup>6</sup>

<sup>1</sup>*Department of Physics and Astronomy, West Virginia University, White Hall, Morgantown, WV 26506, USA; nspol@mix.wvu.edu*

<sup>2</sup>*Center for Gravitational Waves and Cosmology, West Virginia University, Chestnut Ridge Research Building, Morgantown, WV 26505*

<sup>3</sup>*Department of Physics and Astronomy, West Virginia University, P.O. Box 6315, Morgantown, WV 26506, USA*

<sup>4</sup>*Center for Gravitational Waves and Cosmology, West Virginia University, Chestnut Ridge Research Building, Morgantown, WV 26505, USA*

<sup>5</sup>*Jet Propulsion Laboratory, California Institute of Technology, 4800 Oak Grove Drive, Pasadena, CA 91109, USA*

<sup>6</sup>*Department of Astronomy and Cornell Center for Astrophysics and Planetary Science, Cornell University, Ithaca, NY 14853, USA*

### ABSTRACT

We calculate the dispersion measure (DM) contributed by the intergalactic medium (IGM) to the total measured DM for fast radio bursts (FRBs). We use the MareNostrum Instituto de Ciencias del Espacio (MICE) Onion Universe simulation (Fosalba et al.) to track the evolution of the dark matter particle density over a large range of redshifts. We convert this dark matter particle number density to the corresponding free electron density and then integrate it to find the DM as a function of redshift. This approach yields an integrated intergalactic DM of  $DM_{\text{IGM}}(z = 1) = 940^{+8200}_{-200} \text{ pc cm}^{-3}$ , with the large errors representative of the structure in the IGM. We place limits on the redshifts of the current population of observed FRBs. We also use our results to estimate the host galaxy contribution to the DM for the first repeating FRB, FRB 121102, and show that the most probable host galaxy DM contribution,  $DM_{\text{host}} \approx 310 \text{ pc cm}^{-3}$ , is consistent with the estimate made using the Balmer emission lines in the spectrum of the host galaxy,  $DM_{\text{Balmer}} = 324 \text{ pc cm}^{-3}$  (Tendulkar et al.).

*Keywords:* methods: statistical — pulsars: general — galaxies: intergalactic medium

## 1. INTRODUCTION

Fast radio bursts (FRBs) are extragalactic transient radio sources which emit bright ( $\sim$ Jy), millisecond duration bursts. The first FRB was discovered by Lorimer et al. (2007) in archival Parkes Telescope data. Since then, at least an additional 64 FRBs have been detected with different telescopes around the world (Petroff et al. 2016). Of these 65 FRBs, only two, FRB 121102 (Spitler et al. 2014, 2016) and FRB 180814.J0422+73 (The CHIME/FRB Collaboration et al. 2019), are known to have emitted multiple bursts. Out of these two, FRB 121102 has been localized (Chatterjee et al. 2017) to a dwarf galaxy at a redshift of  $z = 0.197$  (Tendulkar et al. 2017), making it unique among all known FRBs.

When FRBs were first discovered (Lorimer et al. 2007; Thornton et al. 2013), it was observed that these bursts had a dispersion measure ( $DM^1$ ) that was significantly higher than the Milky Way contribution to the DM in that direction calculated using the NE2001 Galactic free electron density model (Cordes & Lazio 2002). This led many to believe that these bursts had an extragalactic, if not cosmological, origin. FRB 121102 was confirmed to be of a cosmological origin with the localization and subsequent redshift measurement of  $z = 0.197$  (Tendulkar et al. 2017).

In general, the DM can be calculated by integrating the free electron density,  $n_e(z)$ , along a given line of sight,  $dl$ , up to a redshift  $z_{\max}$  (Ioka 2003; Inoue 2004; Deng & Zhang 2014; McQuinn 2014),

$$DM(z_{\max}) = \int_0^{z_{\max}} \frac{n_e(z)}{1+z} dl, \quad (1)$$

where,

$$dl = c \left| \frac{dt}{dz} \right| dz$$

and

$$\left| \frac{dt}{dz} \right| = \frac{1}{(1+z)H(z)}$$

At very low redshifts,  $z \approx 0$ , for example inside the Milky Way, Eq. 1 reduces to

$$DM = \int_0^L n_e(l) dl, \quad (2)$$

where  $L$  is the distance in parsecs. Note that the free electron density is in units of  $\text{cm}^{-3}$  and the distance has units of parsecs (pc), giving DM the units of  $\text{pc cm}^{-3}$ . The observed DM of an FRB at redshift  $z$ ,  $DM_{\text{obs}}$ , can be split up into the sum of the contributions of its line-of-sight components

$$DM_{\text{obs}}(z) = DM_{\text{ISM}} + DM_{\text{CGM}} + DM_{\text{IGM}}(z) + \frac{DM_{\text{host}}}{1+z}, \quad (3)$$

<sup>1</sup> In this work, we follow the convention from the FRB literature that DM stands for “dispersion measure” and not “dark matter”.

where  $DM_{\text{ISM}}$  represents the contribution from the interstellar medium (ISM) in the Milky Way,  $DM_{\text{CGM}}$  represents the DM contribution from the circumgalactic medium (or halo) around the Milky Way,  $DM_{\text{IGM}}$  represents the DM contribution from the intergalactic medium (IGM), and  $DM_{\text{host}}$  represents the DM contribution from both the interstellar medium in the host galaxy and the local environment of the FRB.

The Milky Way contribution,  $DM_{\text{ISM}}$ , calculated using Eq. 2, can be modeled<sup>2</sup> using the NE2001 Galactic free electron density model (Cordes & Lazio 2002). The circumgalactic medium contribution is usually assumed as  $DM_{\text{CGM}} = 30 \text{ pc cm}^{-3}$  (Dolag et al. 2015), though there will be some directional dependence because of our offset position with respect to the Galactic center. A more detailed modeling of the circumgalactic medium including the directional dependence was done by Prochaska & Zheng (2019a), who found that a better estimate for the dispersion measure contribution from the CGM was  $50 \text{ pc cm}^{-3} < DM_{\text{CGM}} < 80 \text{ pc cm}^{-3}$ . We use the estimate made by Prochaska & Zheng (2019a) in this analysis. This leaves two unknown quantities in Eq. 3, the intergalactic  $DM_{\text{IGM}}$  contribution and the host galaxy  $DM_{\text{host}}$  contribution.

Since the source (or sources) of FRBs are not yet known (see Platts et al. (2018) (and the associated FRB Theory Wiki<sup>3</sup>) for a collection of all source models presented to date), it makes theoretically estimating the local environmental contribution to the total FRB DM difficult. In addition, since FRBs are located at large distances and most have not been localized to a host galaxy, it is extremely difficult to directly probe the environment of the FRB through observations. This makes it hard to develop models which will estimate the value or shape of the DM contribution from the host galaxy of the FRB,  $DM_{\text{host}}$ .

On the other hand, it is relatively straightforward to theoretically derive the IGM’s contribution to the DM using Eq. 1 and assuming a cosmic reionization history (Ioka 2003; Inoue 2004; Deng & Zhang 2014; McQuinn 2014). However, it is difficult to try to observationally constrain the intergalactic DM,  $DM_{\text{IGM}}$ . The delay in the pulse arrival time due to dispersion is inversely proportional to the observing frequency,  $\propto \nu^{-2}$ , the effect of which is observable at radio frequencies. Due to a lack of extragalactic transient sources which are bright enough to be visible in the radio band and narrow enough to allow DM measurements, there had been no empirical measurements of intergalactic DMs outside of the Milky Way and Magellanic Clouds until the discovery of FRBs. In spite of the lack of empirically measured values for  $DM_{\text{IGM}}$ , we can estimate the IGM’s contribution to the total DM measured for FRBs by using Eq. 1.

<sup>2</sup> We do not use the YMW16 model (Yao et al. 2017) in this work because it does not account for local ISM structure nor scattering measurements as part of its fitting, though one can repeat the analysis with this model if desired. Since the observed DMs for FRBs are large and we include errors on the NE2001 values, we do not believe this is an important distinction.

<sup>3</sup> [https://frbtheorycat.org/index.php/Main\\_Page](https://frbtheorycat.org/index.php/Main_Page)

This approach of calculating the intergalactic DM has been performed in quite a few studies, the most popular of which are those by Ioka (2003), Inoue (2004), and McQuinn (2014). Assuming a current free electron density which evolves as  $(1+z)^3$  and different cosmic reionization histories, Ioka (2003) and Inoue (2004) were able to estimate the intergalactic DM out to redshifts as high as  $z = 30$ . Another method makes use of large cosmological simulations to simulate the evolution of the intergalactic medium as a function of redshift. This method was first introduced by Dolag et al. (2015), where they used simulations of the Galactic halo (Beck et al. 2013) to estimate the circumgalactic contribution to the DM for FRBs. They also developed and made use of the *Magneticum Pathfinder*<sup>4</sup> (Dolag et al. 2015) data set to simulate the dark matter and gas particle number density in the universe as a function of redshift. Using these simulations, they were able to produce maps of the free electron density, and thus, the DM as a function of redshift.

The advantages of trying to estimate the intergalactic DM are twofold. One, we can place upper limits on the redshift of the FRBs. If we assume a host galaxy contribution,  $\text{DM}_{\text{host}} = 0$ , then we can solve Eq. 3 for  $\text{DM}_{\text{IGM}}$ , and then use derived intergalactic DM- $z$  relation to place an upper limit on the redshift of the FRB. An example of such an  $\text{DM}_{\text{IGM}}-z$  relation is that derived by Ioka (2003) and Inoue (2004), which at low redshifts ( $z \leq 2$ ) can be expressed as

$$\text{DM}_{\text{IGM}} = 1200 z [\text{pc cm}^{-3}]. \quad (4)$$

Placing such limits on the redshift of the FRBs is useful when performing follow-up studies to locate the host galaxy of the FRB in archival data or estimate the cosmological distribution of the FRBs to, for example, place limits on the baryon mass fraction,  $\Omega_{\text{bary}}$ , or probe the reionization history of the universe (Deng & Zhang 2014). The second advantage of estimating the intergalactic DM is that it allows us to place an estimate on the host galaxy DM distribution. Looking at Eq. 3, we can see that once we know the distribution of  $\text{DM}_{\text{IGM}}$ , we can directly compute the distribution for  $\text{DM}_{\text{host}}$  (within the errors on the estimated Milky Way and halo contributions). This will allow us to probe the region local to the FRB itself. Depending on how constraining the derived  $\text{DM}_{\text{host}}$  distribution is, this might even allow us to rule out some of the proposed source models for FRBs.

In this work, we use cosmological simulations made by the MareNostrum Instituto de Ciencias del Espacio (MICE) team (Fosalba et al. 2008) which simulate the evolution of large scale structure through dark matter particles in a redshift range  $0 < z < 1.4$ . We describe how we convert from the dark matter particle number densities reported in these simulations to baryonic matter density, and then the intergalactic DM in Sec. 2. Next, we develop intergalactic DM probability distributions at different redshifts in Sec. 3. Using these distributions, we place upper limits on the redshifts

for all the observed FRBs in Sec. 4. We exploit the localization of FRB 121102 to a host galaxy at a redshift  $z = 0.192$  (Tendulkar et al. 2017) to place limits on the distribution of the host galaxy DM in Sec. 5. We offer our conclusions in Sec. 6.

In this work, we assume a flat concordance  $\Lambda$ CDM model with the matter density,  $\Omega_m = 0.25$ , dark energy density,  $\Omega_\Lambda = 0.75$ , baryonic matter density,  $\Omega_{\text{bary}} = 0.044$ , and Hubble constant,  $H_0 = 100 h \text{ km s}^{-1} \text{ Mpc}^{-1}$  with  $h = 0.7$ .

## 2. SIMULATIONS

For this analysis, we make use of the MareNostrum Instituto de Ciencias del Espacio (MICE) Onion Universe<sup>5</sup> simulation (Fosalba et al. 2008). This is a large N-body dark matter simulation with  $2048^3$  dark matter particles in a box-size of  $3072 \text{ Mpc}/h$ . The mass of the dark matter particles in this simulation is  $M_{\text{dark}} = 2.34 \times 10^{11} M_\odot/h$ . The output of the simulation is provided in the form of concentric spherical shell lightcones, which are separated by  $\sim 70 \text{ Myr}$ . The maximum radial comoving distance in the simulation is  $\simeq 3 \text{ Gpc}$ , which corresponds to a redshift of  $z \simeq 1.4$ .

This simulation has a much larger volume than the other two best known dark matter simulations, the Millenium simulation (Springel et al. 2005) and the Illustris simulation (Vogelsberger et al. 2014). The MICE Onion Universe simulation also has more dark matter particles than the Illustris simulation, giving a better mass resolution in the simulation. These factors make the MICE Onion simulation best suited for large scale statistical analyses based on the dark matter distribution. The drawback of this simulation is the limited spatial resolution offered in the output dark matter maps. However, this is not a significant issue for our analysis as we are interested in the intergalactic DM contribution and not the DM contribution from individual galaxies or their halos. We note that any intervening halos along the line of sight will contribute to the DM and can do so significantly (Prochaska & Zheng 2019b).

These data were available in the form of HEALPIX maps (Górski et al. 2005), with a resolution defined by  $N_{\text{side}} = 4096$ , providing an angular resolution of  $0.85'$  on the sky. The data set contains the dark matter comoving number density per pixel, in units of  $(\text{Mpc}/h)^{-3}$ . There are a total of 265 such maps corresponding to redshifts ranging from  $0 \lesssim z \lesssim 1.4$ .

### 2.1. Free electron density and dispersion measure

To calculate the contribution to the DM from the IGM, we need to convert the co-moving dark matter number density,  $n_{\text{dark}}(z)$ , in each dark matter map (labeled with subscript  $i$ ) at a sky location given by coordinates  $\phi$  and  $\theta$ , to a comoving free electron density,  $n_e(z)$ ,

$$\begin{aligned} n_e(z_i|\phi, \theta) &= \rho_{\text{bary}}(z_i|\phi, \theta) f_e \\ &= n_{\text{dark}}(z_i|\phi, \theta) \Xi \Upsilon f_e. \end{aligned} \quad (5)$$

<sup>4</sup> <http://www.magneticum.org/>

<sup>5</sup> <http://maia.ice.cat/mice/>

To do this, we first convert the dark matter number density,  $n_{\text{dark}}(z)$ , to the corresponding baryonic matter number density,  $n_{\text{bary}}(z)$ , by using the scaling relation between dark matter and baryonic matter energy density (Komatsu et al. 2011),

$$\Xi \equiv \frac{\Omega_{\text{dark}}}{\Omega_{\text{bary}}} = \frac{24}{4.4} \approx 5.5, \quad (6)$$

where  $\Omega_{\text{dark}}$  and  $\Omega_{\text{bary}}$  are the dark matter and baryonic matter energy density respectively. Since one dark matter particle of the simulation does not correspond to one baryonic matter particle, we need to add an additional “mass factor”,  $\Upsilon$ , to get the baryon matter density,  $\rho_{\text{bary}}(z)$ . Assuming a universe containing only hydrogen and helium, the mass factor is

$$\Upsilon = \frac{M_{\text{dark}}}{(M_{\text{H}} + M_{\text{He}})}, \quad (7)$$

where  $M_{\text{H}}$  and  $M_{\text{He}}$  are the mass of a hydrogen and helium atom respectively.

Next, we convert the baryonic matter number density to a corresponding free electron density. This involves multiplication of the baryonic matter density by an electron ionization fraction,  $f_e$ . Using the formulation presented in Zheng et al. (2014), we define the electron ionization fraction as,

$$f_e = \left[ (1 - Y)f_{\text{HII}} + \frac{1}{4}Y(f_{\text{HeII}} + 2f_{\text{HeIII}}) \right], \quad (8)$$

where  $Y = 0.25$  is the mass fraction of helium,  $f_{\text{HII}}$  is the ionization fraction of hydrogen,  $f_{\text{HeII}}$  and  $f_{\text{HeIII}}$  are the ionization fractions of single and double ionized helium. In this work, we assume that the hydrogen and helium in the IGM are fully ionized, i.e.  $f_{\text{HII}} = f_{\text{HeIII}} = 1$  and  $f_{\text{HeII}} = 0$ . Given our redshift range, we do not expect significant variations in these parameters.

Putting it all together, we obtain Eq. 5 as

$$\begin{aligned} n_e(z_i|\phi, \theta) &= \rho_{\text{bary}}(z_i|\phi, \theta)f_e \\ &= n_{\text{dark}}(z_i|\phi, \theta)\Xi\Upsilon f_e. \end{aligned}$$

Finally, since each map has a finite width in redshift,  $\Delta z$ , we can directly convert the free electron density,  $n_e$ , to the DM in each map,

$$\text{DM}_{\text{map}}(z_i|\phi, \theta) = \frac{n_e(z_i|\phi, \theta)}{1 + z_i} \Delta l(z_i), \quad (9)$$

where the factor of  $(1 + z_i)$  is introduced to account for the redshift in frequencies between the observer and source rest frame (Deng & Zhang 2014), and  $\Delta l(z_i)$  is the comoving width of each map,

$$\Delta l = c \left| \frac{dt}{dz} \right| \Delta z \quad (10)$$

and

$$\begin{aligned} \left| \frac{dt}{dz} \right| &= \frac{1}{(1 + z)H(z)} \\ &= \frac{c \Delta z}{H_0(1 + z)(\Omega_m(1 + z)^3 + \Omega_\Lambda)} \end{aligned} \quad (11)$$

We compute this comoving width for each map using Astropy’s<sup>6</sup> (Astropy Collaboration et al. 2013) Cosmology module. Thus, with the above recipe, we have the DM contribution from the intergalactic medium,  $\text{DM}_{\text{map}}(z_i)$ , at different redshifts. A few examples of these maps are shown in Fig. 1. Finally, to compute the integrated DM,  $\text{DM}_{\text{IGM}}$ , along each line of sight on the sky, we sum the DM contribution of each map out to the desired redshift,

$$\text{DM}_{\text{IGM}}(z|\phi, \theta) = \sum_{i=1}^{z_i=z} \text{DM}_{\text{map}}(z_i|\phi, \theta) \quad (12)$$

### 3. DISPERSION MEASURE STATISTICS

Once we calculate the DM along every line of sight  $(\phi, \theta)$  as given by Eq. 12, we can construct probability distributions for the DM at a given redshift. We will look at two methods of constructing these probability distributions. The first is to create histograms of  $\text{DM}_{\text{IGM}}(z)$  for all values of  $(\phi, \theta)$ . This is equivalent to assuming that the probability of an FRB being on any line of sight is the same. Next, we weight the histograms by assuming that the FRB distribution follows the matter distribution.

#### 3.1. Uniform Weighting

The integrated intergalactic DM probability distributions created by assuming an FRB at the end of every line of sight are shown in the left hand panel of Figure 2. At redshifts  $z \lesssim 0.1$ , the IGM is highly structured, which results in the majority of the sky being devoid of any DM contribution. However, the structures in the IGM contribute significantly larger DMs, even though there are very few regions on the sky that contain these structures. This can be seen in the left-hand panel of Figure 2, where the distributions for  $z \lesssim 0.1$  are heavily concentrated around low values of DM, with the contribution from the IGM structures visible as the outliers at significantly high DM values.

The most probable contributions of the IGM to the DM with uniform weighting as a function of redshift are shown in Fig. 3. The solid blue line represents the peaks of the integrated DM probability distributions shown in Fig. 2, while the blue shaded region represents the 95% confidence region. As we can see, the most probable contribution of the IGM to the DM tends to be very low up to significantly high redshifts. The most probable  $\text{DM}_{\text{IGM}}$  does not exceed  $100 \text{ pc cm}^{-3}$  until a redshift of  $z \sim 0.48$ , while it does not exceed  $1000 \text{ pc cm}^{-3}$  until a redshift of  $z \sim 1.03$ . However, we note that there are significant deviations from these most probable DMs depending on the line of sight along which the FRB might be located, as is evident from the distributions plotted in Fig. 2.

#### 3.2. Weighting by the Matter Distribution

We repeat our analysis by assuming that the probability of an FRB being at the end of a given line of sight is propor-

<sup>6</sup> <http://www.astropy.org>



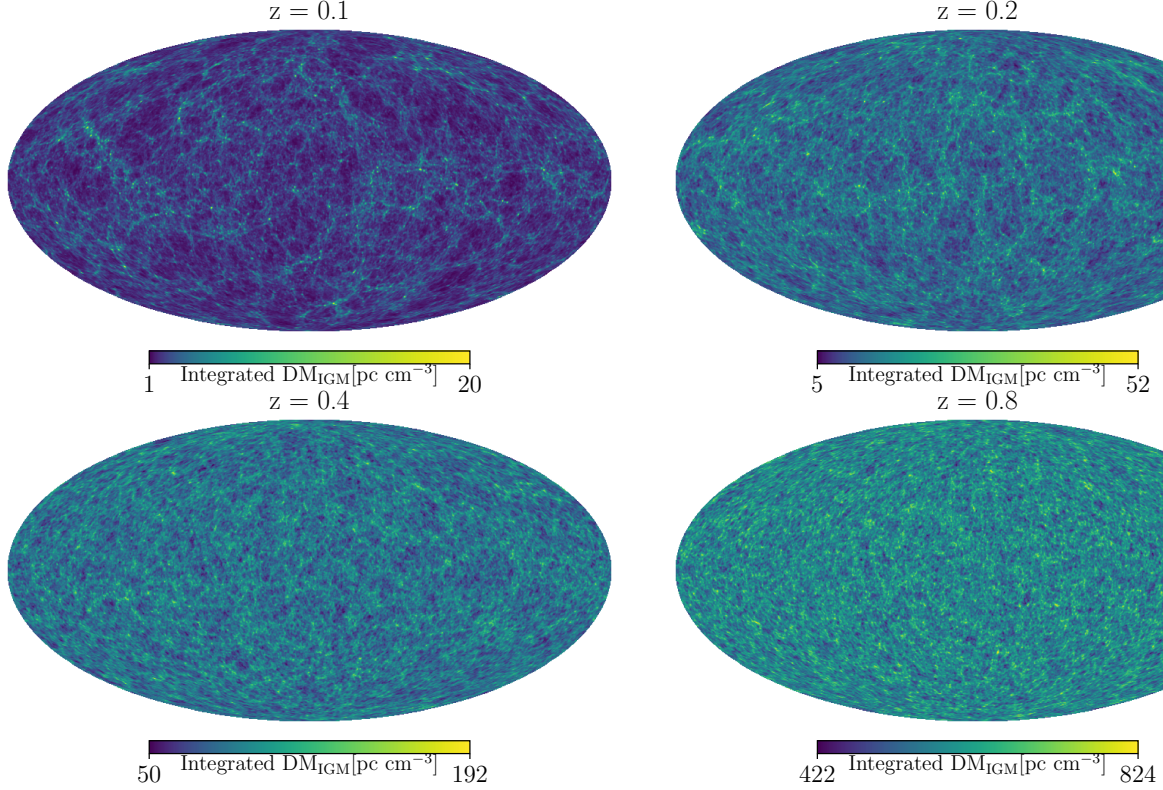


**Figure 1.** The integrated intergalactic DM out to a redshift of  $z = 0.1, 0.2, 0.4, 0.8$ , in the top-left, top-right, bottom-left and bottom-right panels respectively. Notice that the color-bar represents different ranges of the integrated intergalactic DM in each map. We can see that at low redshifts, most of the integrated intergalactic DM contribution is concentrated in filamentary structures on the sky, with the voids on the sky contributing small amounts of DM, which increases as we move to higher redshifts. An animated GIF image is made available with this paper which shows the variation in the integrated  $\text{DM}_{\text{IGM}}$  on the sky with respect to redshift.

tional to the matter density at the final redshift map. That is, rather than add one count to the histogram for each value of  $\text{DM}_{\text{IGM}}(z|\phi, \theta)$ , we add a weight equal to the number of dark matter particles, which is proportional to the dark matter particle number density,  $n_{\text{dark}}(z_i|\phi, \theta)$ . This method assumes that FRBs are more likely to be coincident with higher matter concentrations (e.g., galaxy clusters) and less likely in lower matter concentrations (e.g., voids).

The integrated intergalactic DM probability distributions obtained in this fashion are shown in the right hand panel of Fig 2. We can see that following this approach leads to a much tighter distribution of the possible intergalactic DMs than for the case of uniform weighting. Similarly, we plot the most probable contribution of the IGM under this weighting scheme as the dashed green line in Fig. 3, with the shaded green region representing the 95% confidence region.

As we can see in Fig. 3, the most probable contribution of the intergalactic DM under this weighting scheme closely tracks the contribution obtained under the uniform weighting scheme, but with much tighter constraints on the most probable DM values. The tighter constraints on the upper bounds of the intergalactic DM suggest that this weighting scheme tends to largely ignore the contribution from the structure in the IGM, which is represented by the long tails of the

probability distributions obtained in the uniform weighting scheme. This is to be expected, since the number of pixels, and hence the total number of particles, belonging to the structure at any given redshift are small in number compared to the majority of the pixels which do not belong to this structure. Thus, the relative paucity of these pixels results in them having a smaller overall weight as compared to the pixels which do not belong to the structures. This results in the final PDF de-emphasizing the contribution from the structures, or tails, of the PDF obtained using the uniform weighting scheme.

In the rest of the paper, we report values from both of the weighting schemes wherever it is appropriate.

### 3.3. Comparison with Other $\text{DM}_{\text{IGM}}$ Predictions

A previous estimate of the  $\text{DM}_{\text{IGM}}$  was made by Ioka (2003) and Inoue (2004), whose model predicted a  $\text{DM}_{\text{IGM}}(z = 1) \sim 1200 \text{ pc cm}^{-3}$  (Eq. 4). A similar estimate made by Zhang (2018) predicts  $\text{DM}_{\text{IGM}}(z = 1) \sim 855 \pm 345 \text{ pc cm}^{-3}$ . In comparison, based on our analysis with uniform weighting, we derive a  $\text{DM}_{\text{IGM}}(z = 1) \sim 940^{+8200}_{-200} \text{ pc cm}^{-3}$ , and with weighting by matter distribution, we derive a  $\text{DM}_{\text{IGM}}(z = 1) \sim 960^{+350}_{-160} \text{ pc cm}^{-3}$ , where the errors represent the 95% confidence interval.

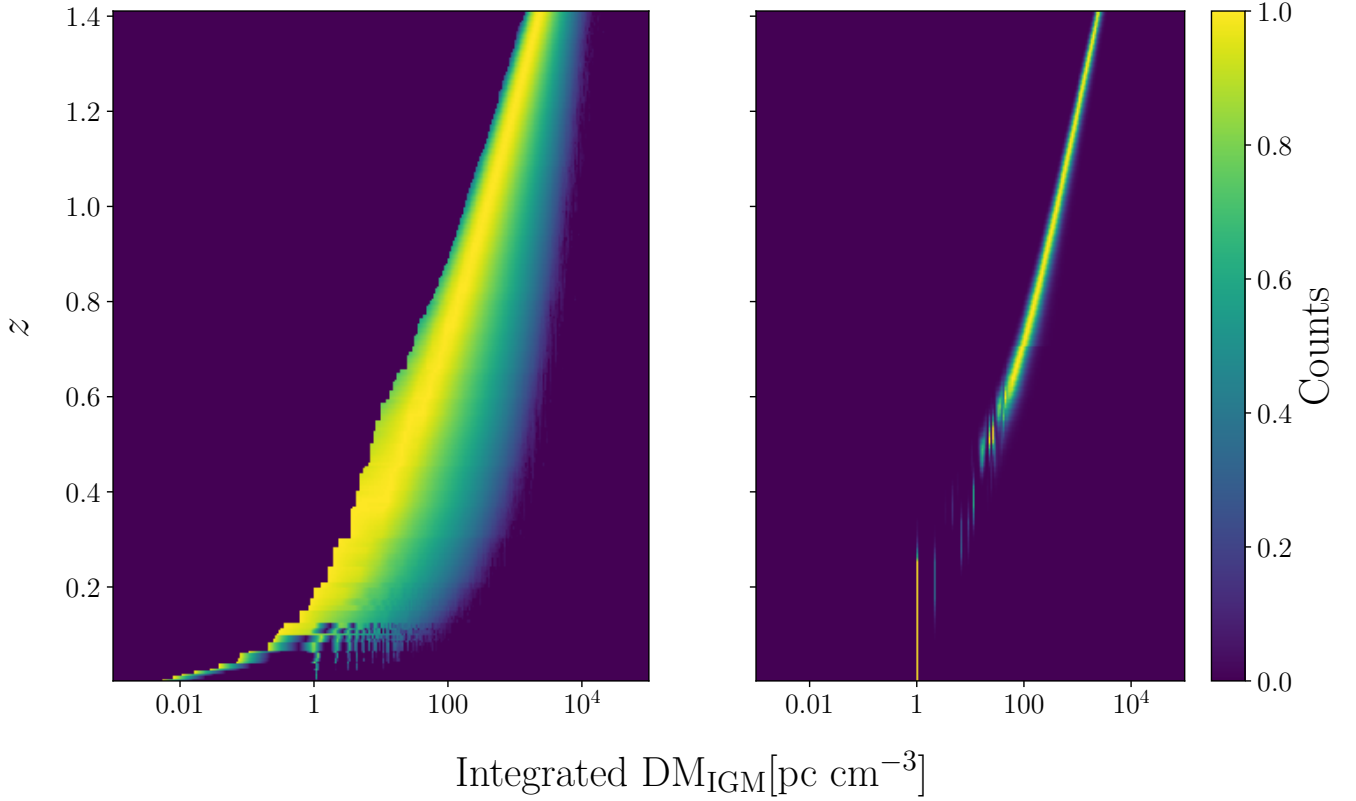


**Figure 2.** The integrated intergalactic DM,  $\text{DM}_{\text{IGM}}$ , PDFs are plotted here as a function of redshift. The left panel represents the PDFs obtained using the uniform weighting scheme, while the right hand panel represents the PDFs obtained using the matter distribution weighting scheme. As described in Sec. 3, the  $\text{DM}_{\text{IGM}}$  is highly structured at redshifts  $z \leq 0.1$ , which results in most of the sky having very low integrated  $\text{DM}_{\text{IGM}}$ . As we move back in redshift, the distribution of  $\text{DM}_{\text{IGM}}$  becomes more uniform across the sky, assuming an almost Gaussian distribution with long trailing edges visible in the uniform weighted PDFs.

The estimates by Ioka (2003), Inoue (2004), and Zhang (2018) relied upon analytical expressions for the evolution of the free electron density,  $n_e(z)$ , as a function of redshift. These analytical expressions track the evolution of the ionization fractions of hydrogen and helium over redshift and are representative of the average behavior of the IGM. Thus, these analyses, unlike ours, do not take into account the spatial variation of the free electron density, and thus the DM, with redshift. In Fig. 3, we compare the results from Ioka (2003) and Inoue (2004) versus the most probable contribution of the IGM to the DM from our analysis.

McQuinn (2014) built upon these works and examined the spatial variation and found that from redshifts 0.5 to 1, the standard deviation about the mean was between 100 and 400  $\text{pc cm}^{-3}$  (which must be multiplied by  $\sim 2$  to arrive at the inner 95% confidence interval assuming Gaussian statistics) both from analytical expressions and also via a 40  $\text{Mpc}/h$ ,  $2 \times 512^3$  dark matter particle cosmological simulation (Faucher-Giguère et al. 2011) to arrive at the baryon distribution for halos along integrated lines of sight.

Another estimate of the intergalactic DM contribution was made by Dolag et al. (2015), where they used the *Magneticum*

*Pathfinder*<sup>7</sup> (Dolag et al. 2015) simulation to simulate the cosmic web, which includes both dark matter and gas matter particles. To compare our results with theirs, we calculate the peaks of their  $\text{DM}_{\text{IGM}}$  (they use the term  $\text{DM}_{\text{cosmo}}$  to represent the same) distributions in the left-hand panel of Fig. 4 using Eqs. 6–10 (see Dolag et al. 2015) and plot them alongside our results in Fig. 3.

As we can see, the other analyses significantly overestimate the IGM contribution to the DM at redshifts  $z < 1$  compared to ours. As a result, estimates of the redshift of the FRB made using these studies would tend to be underestimates as compared to our results. Since redshift predictions usually involve the assumption of  $\text{DM}_{\text{host}} = 0$ , the estimates based on these studies are interpreted as upper limits. Not accounting for the entire possible range of redshifts might lead to follow-up searches not exploring the entire redshift space when searching for the FRB host galaxy in archival data. Another consequence is these other studies would tend to underestimate the host galaxy contribution to the total DM. This might hinder the efforts to understand the local environ-

<sup>7</sup> <http://www.magneticum.org/>

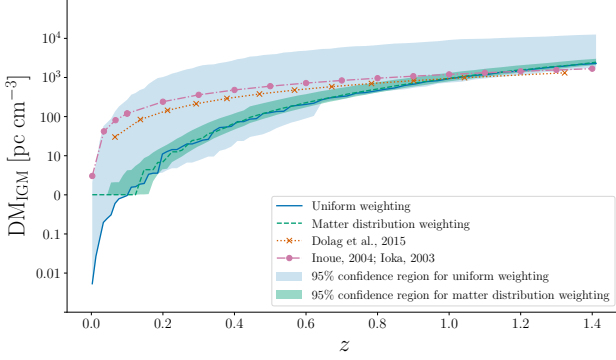


**Figure 3.** The most probable integrated intergalactic DM as a function of redshift. The most probable contribution is the peak of the distributions shown in Fig. 2, with the distributions obtained using the uniform weighting scheme shown as the solid blue line and those obtained using the matter distribution weighting scheme shown as the dashed green lines. The shaded region represents the 95% confidence interval, which is measured starting at the peak of the distribution and collecting 47.5% area on either side of the peak. If the peak of the distribution happens to coincide with the lowest bin, the lower limit on the confidence interval is set to be equal to the value of the peak. For comparison, we also plot the intergalactic DM estimates made by Inoue (2004) and Dolag et al. (2015) as pink dash-dot line and brown dashed lines respectively. We can see that the estimates by Inoue (2004) and Dolag et al. (2015) tend to over-estimate the intergalactic DMs at low redshifts, which in turn underestimates the possible host redshift and DM contribution.

ment of the FRB (or its host galaxy) based on the inferred DM values.

A cosmological-simulation-based estimate of the intergalactic DM contribution was also made by Jaroszynski (2019) using the Illustris simulation (Vogelsberger et al. 2014), where they directly integrated the free electron density over the box size of  $75 \text{ Mpc}/h$ , over a factor of 100 smaller than the MICE Onion simulation used here, though containing baryonic physics. In that study, they report average  $\text{DM}_{\text{IGM}}$  values at different redshifts which are consistent with our results. For example, they predict a  $\text{DM}_{\text{IGM}}(z = 1) = 905 \pm 115 \text{ pc cm}^{-3}$  (error represents one standard deviation), which is consistent with our  $\text{DM}_{\text{IGM}}$  estimate at the same redshift.

We fit the most probable  $\text{DM}_{\text{IGM}}$  as shown in Fig. 3 with a parabolic curve in log-log space and find the functional form to be

$$\log_{10} \text{DM} = 0.48(\log_{10} z)^2 + 3.34(\log_{10} z) + 2.98 \quad (13)$$

where DM is in units of  $\text{pc cm}^{-3}$ .

We used the uniform-weighting curve because it avoids the flattening at  $z \lesssim 0.1$ , though qualitatively the curves match quite well at all higher redshifts. This equation can be used to extrapolate to higher redshifts though of course care should be taken in doing so.

### 3.4. IGM DM contribution under 100 Mpc

The galaxy clusters closest to the Milky Way, such as the Virgo, Fornax and Hydra clusters (Abell et al. 1989), lie within 100 Mpc ( $z = 0.023$ , Wright 2006) of the Milky Way. The intergalactic DM contribution at these low redshifts is small relative to the contribution from the Milky Way and the host galaxy. For example, the Milky Way ISM contribution (not including the halo contribution) in the direction of the Virgo cluster, which is at a distance of approximately 20 Mpc ( $z \approx 0.004$ , Wright 2006), is  $\text{DM}_{\text{ISM}} \approx 30 \text{ pc cm}^{-3}$  (Cordes & Lazio 2002), while the intergalactic DM contribution is  $\text{DM}_{\text{IGM}} < 4 \text{ pc cm}^{-3}$ .

Because of these low DMs involved, care must be taken about the range of DMs over which FRBs are searched for in these nearby clusters.

## 4. REDSHIFT LIMITS ON FAST RADIO BURSTS

One application of this analysis is in deriving redshift limits for the observed FRBs. Using Eq. 3, we can calculate the empirical  $\text{DM}_{\text{IGM}}$ ,

$$\text{DM}_{\text{IGM}}(z) = \text{DM}_{\text{obs}} - \text{DM}_{\text{ISM}} - \text{DM}_{\text{CGM}} - \frac{\text{DM}_{\text{host}}}{1 + z} \quad (14)$$

Given the lack of modeling of the host galaxy DM, we assume  $\text{DM}_{\text{host}} = 0 \text{ pc cm}^{-3}$  for now. This implies that the redshift limits we derive will be upper limits.

We can compute the joint probability distribution function (PDF),  $f(\text{DM}_{\text{IGM}}, z)$ , by normalizing the two dimensional histogram shown in Fig. 3. Using this joint PDF and an intergalactic DM,  $\text{DM}_{\text{IGM}}$ , deduced from Eq. 14, we can estimate the probability,  $f(z|\text{DM}_{\text{IGM}})$ , that the FRB lies at a redshift,  $z$ , by

$$\begin{aligned} f(\text{DM}_{\text{IGM}}, z) &= f(z|\text{DM}_{\text{IGM}}) \times f(\text{DM}_{\text{IGM}}) \\ \Rightarrow f(z|\text{DM}_{\text{IGM}}) &= \frac{f(\text{DM}_{\text{IGM}}, z)}{f(\text{DM}_{\text{IGM}})}, \end{aligned} \quad (15)$$

where  $f(\text{DM}_{\text{IGM}})$  accounts for the error on the intergalactic DM deduced from Eq. 14, which includes the error on the measured total DM and the Milky Way contribution to the DM and therefore includes the observational uncertainties along with the uncertainties from the Milky Way electron density model and the CGM. While in NE2001, the typical distance error is  $\approx 20\%$  for an object with a given DM (Cordes & Lazio 2002), we use a 20% error on the Milky Way's DM contribution to be conservative. For the Halo contribution, we use the 50-80  $\text{pc cm}^{-3}$  range from Prochaska & Zheng (2019a) and then assume that the Halo contribution is  $65 \pm 15 \text{ pc cm}^{-3}$ . For all three values, we assume that the probabilities are given by a Gaussian distribution with standard deviation equal to the appropriate errors. Then, using Eq. 15, we place upper limits on the redshifts of the FRBs using both the uniform weighting and matter distribution weighting, shown in Fig. 4.

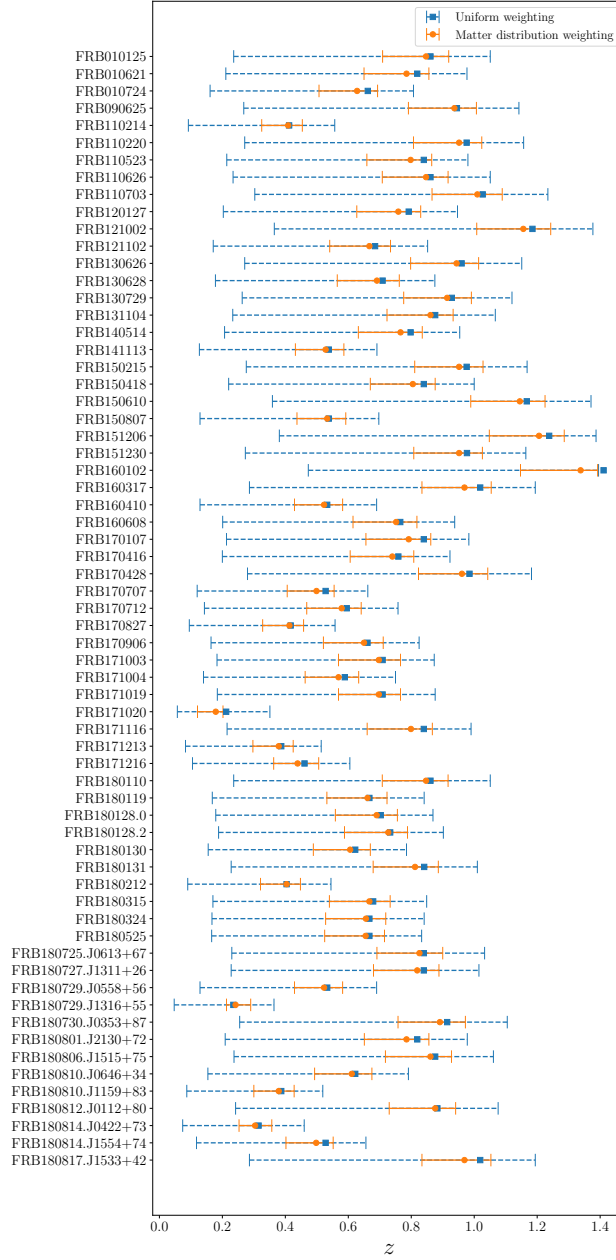


**Figure 4.** The 95% redshift upper limits on all currently known FRBs using our model of the intergalactic DM, as described in Sec. 4, assuming  $\text{DM}_{\text{host}} = 0$ . The redshift limits based on the uniform weighting scheme are shown in blue, while those based on the matter distribution weighting scheme are shown in orange. These predicted redshifts imply that all FRBs detected so far are likely to be extragalactic sources. While we can place constraining limits on the redshifts of other FRBs, we note that the DM measured for FRB 160102 is high enough that we can only place a lower limit on the possible redshift of this source.

As expected, the redshift limits predict that all known FRBs are likely of extragalactic or cosmological origin. The limits predicted using matter distribution weighting are much tighter than those predicted using uniform weighting. This is because the intergalactic DM distributions generated using the matter distribution weighting scheme are much narrower. Similarly, the larger errors on the redshifts predicted using uniform weighting, especially those towards lower redshifts,

are a result of the long tails of the intergalactic DM PDFs shown in Fig. 2. In our opinion, the redshifts predicted using the matter distribution weighting can be used as upper limits for any given FRB.

We can compare our redshift limits for FRB 121102 which is the only FRB which has a measured spectroscopic redshift ( $z = 0.1927$ , [Tendulkar et al. 2017](#)). Using the uniform weighting scheme for the intergalactic DM distribution, we



predict a redshift range of  $z_{121102, \text{uniform}} = 0.68^{+0.17}_{-0.52}$ , while using the matter distribution weighting scheme, we predict a redshift limit of  $z_{121102, \text{matter}} = 0.67^{+0.07}_{-0.13}$ . Both the weighting schemes predict a redshift higher than the true redshift of FRB 121102, which is to be expected since these predictions assume a host contribution of  $\text{DM}_{\text{host}} = 0 \text{ pc cm}^{-3}$ . As we show in Sec. 5, the host galaxy contribution for FRB 121102 (and probably all FRBs) is significant. Thus, we can treat  $z_{121102} \leq 0.74$  as an upper limit on the redshift of FRB 121102.

We can then compare our redshift upper limits to those made in other works, especially those by Ioka (2003); Inoue (2004) who predict an upper limit of  $z \leq 0.32$ . Accounting for the variance in mapping the DM to redshift (McQuinn 2014) increases this upper limit to  $z \leq 0.42$ . These upper limit predictions are smaller than those that we make in this work and might result in searches for the host galaxy in archival data not exploring the entire possible redshift space.

Thus, our limits can be used to eliminate potential host galaxies that fall above our predicted upper limit on the redshift and can reduce the time required to search for a host galaxy. This will be useful for large field-of-view surveys which do not have arcsecond localization capabilities and thus have lots of potential host galaxies in their field-of-view, for example, the Canadian HI Intensity Mapping Experiment (CHIME) FRB experiment (The CHIME/FRB Collaboration et al. 2018). We provide Python scripts to generate the probable redshift of an FRB given its total DM and position on the sky in the GitHub repository<sup>8</sup> associated with this work.

## 5. ESTIMATING THE HOST GALAXY DISPERSION MEASURE

Another application of this work is to allow direct estimates of the host galaxy DM contribution,  $\text{DM}_{\text{host}}$ , if the redshift of the FRB, and thus the host galaxy, is known. Again using Eq. 3, we can directly calculate the PDF for the DM of the host galaxy,

$$\text{DM}_{\text{host}} = (\text{DM}_{\text{obs}} - \text{DM}_{\text{ISM}} - \text{DM}_{\text{CGM}} - \text{DM}_{\text{IGM}})(1+z) \quad (16)$$

This  $\text{DM}_{\text{host}}$  PDF is a sum of the DM local to the source of the FRB and the DM contributed by the interstellar medium in the rest of the host galaxy along the line of sight. For non-repeating FRBs, the observed DM,  $\text{DM}_{\text{obs}}$  will be a single measured value, while for repeating FRBs,  $\text{DM}_{\text{obs}}$  will be a distribution depending on the variation of the total measured DM at different epochs. These short-timescale DM variations are likely to be local to the source of the FRB and will be reflected as a broadening in the  $\text{DM}_{\text{host}}$  PDF calculated using Eq. 16.

The PDFs of the different contributions to the DM are shown in Fig. 5 using the example of FRB 121102 (Spitler et al. 2014). Multiple bursts ( $\sim 100$ ) have now been de-

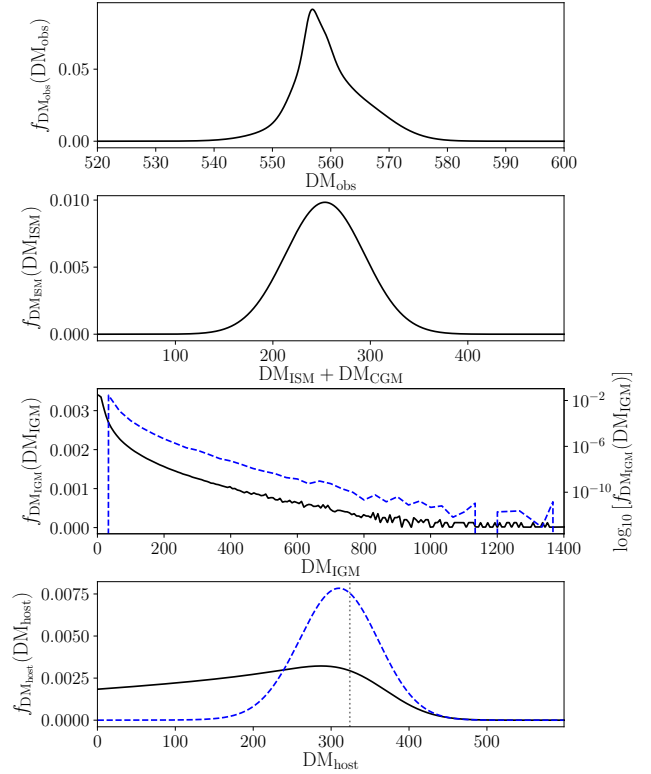


**Figure 5.** *Top panel:* The distribution of the observed total DM for FRB 121102 generated using the DMs reported in Spitler et al. (2016) and Scholz et al. (2016). *Second panel:* The sum of the Milky Way (Cordes & Lazio 2002) and circumgalactic medium (halo, Prochaska & Zheng 2019a) contributions to the total DM for FRB 121102. We assume a 20% error on the Milky Way contribution to the total DM, while we assume a circumgalactic DM contribution of  $65 \pm 15 \text{ pc cm}^{-3}$ . *Third panel:* The intergalactic DM from the redshift slice at  $z = 0.192$  (Tendulkar et al. 2017) generated in this work, where the black now denotes the uniform weighting distribution and the dashed blue lines show the distributions using the matter distribution weighting. Note the wide range of scales involved for the matter distribution weighted distribution, shown on a logarithmic axis on the right. *Bottom panel:* The host galaxy DM contribution to the total DM. This is obtained by subtracting the Milky way, circumgalactic, and IGM DM distributions from the total DM distribution. As before, the dashed blue line represents the PDF of the matter distribution weighted distribution, though now on a linear scale. The dotted gray line shows the Balmer-line-derived DM of  $324 \text{ pc cm}^{-3}$  (Tendulkar et al. 2017). Note the varying scales on the horizontal axes and that the units are all in the standard  $\text{pc cm}^{-3}$ .

tected from FRB 121102 (for example, Scholz et al. 2016; Gajjar et al. 2018; Zhang et al. 2018). All the bursts have been observed with an average DM,  $\text{DM}_{\text{obs}} = 557 \text{ pc cm}^{-3}$ , though different bursts have shown different DMs (Spitler et al. 2016; Scholz et al. 2016). Even accounting for the time-frequency structures of the bursts and correcting the

<sup>8</sup> [https://github.com/NihanPol/DM\\_IGM](https://github.com/NihanPol/DM_IGM)

DMs, [Hessels et al. \(2018\)](#) find true DM variations over time as well. We combine the DMs reported for FRB 121102 in [Spitler et al. \(2016\)](#) and [Scholz et al. \(2016\)](#) to produce the conservative distribution of the observed DM given their wide spread and the use of determining the DM from the peak signal-to-noise ratio for the bursts; this distribution is shown in the top panel of Fig. 5.

We compute the Milky Way contribution using the NE2001 model ([Cordes & Lazio 2002](#)) which turns out to be  $188 \text{ pc cm}^{-3}$ . We again assume a 20% error associated with this Galactic DM contribution ([Cordes & Lazio 2002](#)) and a circumgalactic DM contribution of  $65 \pm 15 \text{ pc cm}^{-3}$  to the Galactic DM to get the total DM contribution from the Milky Way, i.e.  $\text{DM}_{\text{ISM}} + \text{DM}_{\text{CGM}}$ , which is shown in the second panel in Fig. 5. Finally, using the fact that FRB 121102 lies at a redshift of  $z = 0.192$ , we choose the map at this redshift and use the PDF of the  $\text{DM}_{\text{IGM}}$ , both with uniform and matter distribution weighting, in this map as the intergalactic DM contribution. These PDFs of  $\text{DM}_{\text{IGM}}$  are shown in the third panel in Fig. 5. Given these distributions, we can calculate the host galaxy contribution to the DM using Eq. 16. The host galaxy DM,  $\text{DM}_{\text{host}}$ , so obtained is shown in the bottom panel of Fig. 5.

As shown, we derive a broad range of possible  $\text{DM}_{\text{host}}$ , with the most probable contribution for the uniform weighting scheme being  $\approx 290 \text{ pc cm}^{-3}$ , with an upper limit of  $380 \text{ pc cm}^{-3}$  at the 95% confidence level. For the matter distribution weighting, we find that  $\text{DM}_{\text{host}} = 310 \pm 50 \text{ pc cm}^{-3}$ . The latter is inconsistent with the estimates of [Yang et al. \(2017\)](#), where they estimated that host contribution was  $210 \text{ pc cm}^{-3}$ . However, they assumed a Halo contribution of  $30 \text{ pc cm}^{-3}$  and therefore comparing to our estimates using  $\approx 65 \text{ pc cm}^{-3}$ , their estimates are well below ours. As seen in Fig. 5, we find that both of our values are consistent with that calculated using the Balmer emission lines in the spectrum of the host galaxy. Converting the emission measure ( $\text{EM} = \int n_e^2(l) dl$ ) to a DM by assuming strong variations in the electron density, [Tendulkar et al. \(2017\)](#) approximate the host of FRB 121102 to have  $\text{DM}_{\text{Balmer}} = 324 \text{ pc cm}^{-3}$ , though this value is highly uncertain due to the unknown nature of the host environment.

We can instead invert the analysis to constrain properties of the host galaxy medium. Following [Tendulkar et al. \(2017\)](#) (see also [Cordes et al. 1991, 2016](#)), we have that the DM value of the host galaxy with total path length  $L$  should be

$$\text{DM}_{\text{host}} \approx 774 \text{ pc cm}^{-3} \left( \frac{L}{4 \text{ kpc}} \right)^{1/2} \times \left[ \frac{f}{\zeta(1 + \epsilon^2)/4} \right]^{1/2} \left( \frac{\text{EM}_{\text{host}}}{600 \text{ pc cm}^{-6}} \right)^{1/2} \quad (17)$$

where  $f$  is the filling factor of ionizing material in structures (e.g., clouds),  $\zeta = \langle n_e^2 \rangle / \langle n_e \rangle^2$  describes the electron-density variations between structures ( $\zeta = 2$  for 100% variations), and  $\epsilon$  is the fractional density fluctuation (root-mean-square density divided by the mean density) within structures ( $\epsilon =$

1 for fully modulated). The fiducial value for  $\text{EM}_{\text{host}} \approx 600 \text{ pc cm}^{-6}$  comes from the measurement in [Tendulkar et al. \(2017\)](#), as does the size of 4 kpc given the maximum diameter extent of the host galaxy they measure. Given our estimate of  $\text{DM}_{\text{host}} = 310 \text{ pc cm}^{-3}$ , we then have that

$$\frac{f}{\zeta(1 + \epsilon^2)/4} \approx 0.16. \quad (18)$$

Since by definition  $f$  and  $\epsilon$  cannot be greater than unity, and  $\zeta$  must be greater than unity, then the filling factor along the line of sight must be  $\lesssim 64\%$  though it will likely be much less.

## 6. CONCLUSION

In this work, we have calculated the DM contribution from the IGM using large scale cosmological dark matter simulations. We predict lower values of intergalactic DMs at low redshifts than those predicted by other works such as [Ioka \(2003\)](#), [Inoue \(2004\)](#), and [Dolag et al. \(2015\)](#). Using our PDFs for the intergalactic DM contribution at different redshifts, we set upper limits on the redshifts of all the observed FRBs. The predicted redshifts are large enough that we can conclude FRBs to be extragalactic sources. Using the example of the localization of FRB 121102, we demonstrate how our intergalactic DM PDFs can be used to place constraints on the DM contribution of the host galaxy and local environment of the FRB and show that they are consistent with the DM measured using Balmer emission lines in the spectrum of the host galaxy.

Localization of FRBs, either through instantaneous high-time-resolution transient imaging (e.g., *realfast*; [Law et al. 2018](#), or the DSA110; [Ravi 2018](#)) or interferometric detection of repeaters as with FRB 121102, will allow for the determination of redshifts to FRB hosts, in which case we can use our results to place limits on the host contribution to the total dispersion measure. In the cases of other large-scale FRB surveys where localization is not immediately obtained, such as with CHIME, SUPERB at Parkes ([Bhandari et al. 2018](#)), and UTMOST ([Caleb et al. 2016, 2017](#)), our work provides constraints on the redshifts of FRBs. We have found that nearly all discovered FRBs so far have  $z \lesssim 1$ , though as new surveys are searching over a larger range of DMs, we will need to extrapolate our results either from the redshifts we have integrated over so far or from the properties of the cosmic web simulations themselves and then integrating farther in redshift space.

We would like to thank the MICE team, who were kind enough to provide us full access to the Onion universe data.

MAM, MTL, NP, TJWL and JMC are members of the NANOGrav Physics Frontiers Center (NSF PHY-1430284). MAM and NP are supported by NSF AAG-1517003. MAM also has additional support from NSF OIA-1458952. Part of this research was carried out at the Jet Propulsion Laboratory, California Institute of Technology, under a contract with the National Aeronautics and Space Administration.

## REFERENCES

- Abell, G. O., Corwin, Jr., H. G., & Olowin, R. P. 1989, *ApJS*, 70, 1
- Astropy Collaboration, Robitaille, T. P., Tollerud, E. J., et al. 2013, *A&A*, 558, A33
- Beck, A. M., Dolag, K., Lesch, H., & Kronberg, P. P. 2013, *MNRAS*, 435, 3575
- Bhandari, S., Keane, E. F., Barr, E. D., et al. 2018, *MNRAS*, 475, 1427
- Caleb, M., Flynn, C., Bailes, M., et al. 2016, *MNRAS*, 458, 718
- . 2017, *MNRAS*, 468, 3746
- Chatterjee, S., Law, C. J., Wharton, R. S., et al. 2017, *Nature*, 541, 58
- Cordes, J. M., & Lazio, T. J. W. 2002, arXiv e-prints, astro
- Cordes, J. M., Weisberg, J. M., Frail, D. A., Spangler, S. R., & Ryan, M. 1991, *Nature*, 354, 121
- Cordes, J. M., Wharton, R. S., Spitler, L. G., Chatterjee, S., & Wasserman, I. 2016, arXiv e-prints, arXiv:1605.05890
- Deng, W., & Zhang, B. 2014, *ApJL*, 783, L35
- Deng, W., & Zhang, B. 2014, *The Astrophysical Journal*, 783, L35
- Dolag, K., Gaensler, B. M., Beck, A. M., & Beck, M. C. 2015, *MNRAS*, 451, 4277
- Faucher-Giguère, C.-A., Kereš, D., & Ma, C.-P. 2011, *MNRAS*, 417, 2982
- Fosalba, P., Gaztañaga, E., Castander, F. J., & Manera, M. 2008, *MNRAS*, 391, 435
- Gajjar, V., Siemion, A. P. V., Price, D. C., et al. 2018, *ApJ*, 863, 2
- Górski, K. M., Hivon, E., Banday, A. J., et al. 2005, *ApJ*, 622, 759
- Hessels, J. W. T., Spitler, L. G., Seymour, A. D., et al. 2018, arXiv e-prints, arXiv:1811.10748
- Inoue, S. 2004, *MNRAS*, 348, 999
- Ioka, K. 2003, *ApJL*, 598, L79
- Jaroszynski, M. 2019, *MNRAS*, 11
- Komatsu, E., Smith, K. M., Dunkley, J., et al. 2011, *The Astrophysical Journal Supplement Series*, 192, 18
- Law, C. J., Bower, G. C., Burke-Spolaor, S., et al. 2018, *The Astrophysical Journal Supplement Series*, 236, 8
- Lorimer, D. R., Bailes, M., McLaughlin, M. A., Narkevic, D. J., & Crawford, F. 2007, *Science*, 318, 777
- McQuinn, M. 2014, *The Astrophysical Journal Letters*, 780, L33
- Petroff, E., Barr, E. D., Jameson, A., et al. 2016, *PASA*, 33, e045
- Platts, E., Weltman, A., Walters, A., et al. 2018, arXiv e-prints, arXiv:1810.05836
- Prochaska, J. X., & Zheng, Y. 2019a, *MNRAS*, 258
- . 2019b, *MNRAS*, arXiv:1901.11051
- Ravi, V. 2018, arXiv e-prints, arXiv:1804.07291
- Scholz, P., Spitler, L. G., Hessels, J. W. T., et al. 2016, *ApJ*, 833, 177
- Spitler, L. G., Cordes, J. M., Hessels, J. W. T., et al. 2014, *ApJ*, 790, 101
- Spitler, L. G., Scholz, P., Hessels, J. W. T., et al. 2016, *Nature*, 531, 202
- Springel, V., White, S. D. M., Jenkins, A., et al. 2005, *Nature*, 435, 629
- Tendulkar, S. P., Bassa, C. G., Cordes, J. M., et al. 2017, *ApJL*, 834, L7
- The CHIME/FRB Collaboration, Amiri, M., Bandura, K., et al. 2018, *The Astrophysical Journal*, 863, 48
- The CHIME/FRB Collaboration, :, Amiri, M., et al. 2019, arXiv e-prints, arXiv:1901.04525
- Thornton, D., Stappers, B., Bailes, M., et al. 2013, *Science*, 341, 53
- Vogelsberger, M., Genel, S., Springel, V., et al. 2014, *MNRAS*, 444, 1518
- Wright, E. L. 2006, *PASP*, 118, 1711
- Yang, Y.-P., Luo, R., Li, Z., & Zhang, B. 2017, *ApJL*, 839, L25
- Yao, J. M., Manchester, R. N., & Wang, N. 2017, *ApJ*, 835, 29
- Zhang, B. 2018, *ApJL*, 867, L21
- Zhang, Y. G., Gajjar, V., Foster, G., et al. 2018, *ApJ*, 866, 149
- Zheng, Z., Ofek, E. O., Kulkarni, S. R., Neill, J. D., & Juric, M. 2014, *ApJ*, 797, 71